Retrieval of Snow Properties for Ku- and Ka-Band Dual-Frequency Radar

LIANG LIAO

Goddard Earth Science Technology and Research Program, Morgan State University, Baltimore, Maryland

ROBERT MENEGHINI

NASA Goddard Space Flight Center, Greenbelt, Maryland

ALI TOKAY

University of Maryland, Baltimore County, and Joint Center for Earth Systems Technology, Baltimore, Maryland

LARRY F. BLIVEN

NASA Wallops Flight Facility, Wallops Island, Virginia

(Manuscript received 9 December 2015, in final form 10 June 2016)

ABSTRACT

The focus of this study is on the estimation of snow microphysical properties and the associated bulk parameters such as snow water content and water equivalent snowfall rate for Ku- and Ka-band dual-frequency radar. This is done by exploring a suitable scattering model and the proper particle size distribution (PSD) assumption that accurately represent, in the electromagnetic domain, the micro-/macrophysical properties of snow. The scattering databases computed from simulated aggregates for small-to-moderate particle sizes are combined with a simple scattering model for large particle sizes to characterize snow-scattering properties over the full range of particle sizes. With use of the single-scattering results, the snow retrieval lookup tables can be formed in a way that directly links the Ku- and Ka-band radar reflectivities to snow water content and equivalent snowfall rate without use of the derived PSD parameters. A sensitivity study of the retrieval results to the PSD and scattering models is performed to better understand the dual-wavelength retrieval uncertainties. To aid in the development of the Ku- and Ka-band dual-wavelength radar technique and to further evaluate its performance, self-consistency tests are conducted using measurements of the snow PSD and fall velocity acquired from the Snow Video Imager/Particle Image Probe (SVI/PIP) during the winter of 2014 at the NASA Wallops Flight Facility site in Wallops Island, Virginia.

1. Introduction

The Global Precipitation Measurement (GPM) core satellite, a joint Earth-observing mission between the National Aeronautics and Space Administration (NASA; see the appendix for a list of key acronyms and symbols used in this article) and the Japan Aerospace Exploration Agency (JAXA), was successfully launched into orbit on 27 February 2014 from Japan (Hou et al. 2008, 2014). One of the goals of the Dual-Frequency Precipitation Radar (DPR) aboard the GPM satellite is to provide measurements and estimates of snow precipitation rate and water content for mid- and high-latitude regions. This is usually done by estimating parameters of the snow particle size distribution (PSD) that are often modeled by an analytical function, such as the exponential, gamma, or lognormal distribution, with two or three unknown parameters (Gorgucci et al. 2000, 2002; Bringi et al. 2002). The inability of the modeled PSD to represent actual snow spectra and to characterize their intrinsic variations in time and space can lead to errors in the estimates of the precipitation rate obtained from the DPR. Additionally, uncertainties associated with scattering computations of snow aggregates also affect the accuracy of the dual-wavelength radar retrieval of

Corresponding author address: Dr. Liang Liao, NASA Goddard Space Flight Center, Code 612, Greenbelt, MD 20771.
E-mail: liang.liao-1@ nasa.gov

snow arising from the complex shape and structure of snow aggregates and the corresponding variability in the scattering parameters. Therefore, understanding the uncertainties in snow precipitation estimation that depend on PSD parameterizations and scattering models of individual particles is important in evaluating the overall performance of DPR retrieval algorithms and in gaining insights into ways to improve the algorithms.

Several studies have been carried out using dual-frequency radar for the retrieval of precipitating ice/snow parameters from the ground (Matrosov 1998; Szyrmer and Zawadzki 2014a,b) and from airborne radar measurements (Liao et al. 2005, 2008; Heymsfield et al. 2005; Wang et al. 2005; Matrosov et al. 2005). Although various combinations of frequencies were used in these studies, a common feature is that at least one of the radar frequencies operates in the non-Rayleigh regime to ensure a measurable difference in the reflectivities. It is this differential reflectivity that can be related to a characteristic size parameter of the snow particle distribution. Because of uncertainties in the snow microphysics arising from the natural variability of the particle density, shape, and orientation, and also because of uncertainties associated with the particle-backscattering cross section and terminal fall velocity, as well as the natural variability in PSDs, it is important to assess the errors in the model and their impacts on the retrievals.

The emphasis of this study is on the estimation of snow microphysical properties and the associated bulk parameters such as snow water content and water equivalent snowfall rate. As indicated earlier, one of the challenges in the radar retrieval of snow is to characterize the variability of the snow PSD and to efficiently compute scattering properties of the snowflakes over the full range of sizes. The aim of our study is to explore a suitable scattering model and an appropriate PSD that accurately represents, in the electromagnetic domain, the micro-/macrophysical properties of snow.

Although several scattering databases are available, which provide the scattering properties of snow aggregates (Liu 2004, 2008; Nowell et al. 2013; Kuo et al. 2016), they are often limited to small-to-moderate particle sizes for a limited set of frequencies. These limitations arise not only because of the magnitude of the computational burden but also because of the convergence properties of the numerical solution. To develop an operational-type radar algorithm for the DPR snow retrieval, it is desirable to have a scattering model that provides efficient computation at an arbitrary frequency over a large range of particle sizes. Comparisons of the scattering results between simple

and more complicated snow models indicate that the scattering properties of aggregates at the DPR frequencies are fairly well reproduced by randomly oriented ellipsoidal particles if the effective mass density of snow is constant with size (Liao et al. 2013). By taking advantage of both developed scattering databases and simple scattering models, we attempt to employ the scattering results of the aggregates from the scattering database for small to moderate particle sizes and use the results from the simple scattering models for large particles to cover the full range of particle sizes for characterizing the snow-scattering properties at Ku and Ka bands.

One of the DPR algorithms for snow retrieval employs a fixed-snow-density spherical model for computations of the Ku- and Ka-band radar backscattering and extinction cross sections using the assumption of an exponential PSD (Seto et al. 2013). To improve snow retrieval accuracy, we will investigate retrieval uncertainties associated with the PSD and the particle-scattering models, and introduce new forms of the retrieval lookup tables that directly link DPR Ku- and Ka-band radar reflectivities to snow water content and snowfall rate without the use of derived PSD parameters. Newly formed lookup tables provide an effective means not only for snow retrieval but also for analysis of the retrieval uncertainties associated with the PSD model and the particle-scattering models. To check the consistency of the snow retrievals, measurements of the snow PSD and fall velocity acquired from the Snow Video Imager/Particle Image Probe (SVI/PIP) are used (Newman et al. 2009). It is believed that a collection of long-term PSD data, fall velocities, and information on particle mass spectra will provide a strong basis for evaluating the performance of the DPR Ku- and Ka-band techniques.

This article is organized as follows. Methods for snow retrieval are described in section 2, and measurements of the PSD are discussed in section 3, followed by remarks and a summary in section 4.

2. Technical approach and methodology

Understanding the retrieval errors associated with the snow particle size/mass distributions models and particle-scattering models employed by the DPR algorithms is important for the evaluation of algorithm performance. The study also provides insight into which of the models yield the most accurate DPR estimates of snow. Proper selection of the PSD and scattering models can improve the overall performance of the DPR profiling algorithm. What follows are discussions of snow-scattering models and the parameterization of the
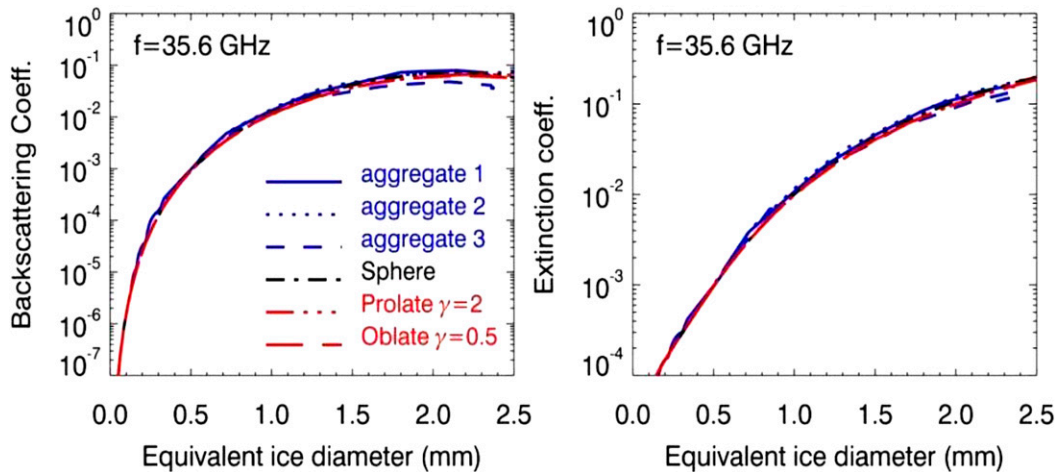
FIG. 1. Comparisons of (left) backscattering and (right) extinction coefficients of three snow aggregates with the results from the sphere, oblate, and prolate spheroids at a frequency of 35.6 GHz in terms of equivalent ice diameter. A constant snow density of $0.2 \, \mathrm{g \, cm^{-3}}$ is assumed for all spherical and spheroidal particle models. The oblate and prolate spheroids are randomly oriented with γ of 0.5 and 2, respectively.

particle size spectra and how these models affect the radar retrievals.

a. Single-scattering model of snow aggregates

Several simulated aggregate models have been developed using the pristine ice crystal habits found in nature as the basic elements from which the aggregates are constructed (Draine and Flatau 1994; Liu 2004, 2008; Weinman and Kim 2007; Petty and Huang 2010; Botta et al. 2010 and 2011; Nowell et al. 2013; Kuo et al. 2016). For these particles, a numerical scheme is required to compute the scattered fields. Although these numerical computations are useful, they are time consuming and are often limited to small-to-moderate particle sizes for a limited set of frequencies. A few scattering databases derived from simulated aggregates are available (Nowell et al. 2013; Kuo et al. 2016), but the maximum equivalent ice diameter is limited to around 2.5–3 mm, which is not large enough to cover the entire particle size range.

To account for the scattering contribution from the entire particle size range, the current DPR algorithms adopt a simple scattering model, namely, the ice–air mixed spheres with a fixed snow density of $0.1 \, \mathrm{g \, cm^{-3}}$ for all particle sizes (Seto et al. 2013). To check the validity and accuracy of the simple geometric scattering model, a study was carried out by Liao et al. (2013) in which scattering results from aggregates composed of six-branch bullet-rosette crystals were compared with those obtained from spherical or spheroidal ice–air mixed-phase particles. Shown in Fig. 1 is an example of these results, in which backscattering (left) and extinction (right) coefficients at 35.6 GHz are plotted

versus the equivalent ice diameter for three simulated snow aggregates and results from the sphere, oblate, and prolate spheroids. A constant effective snow density of $0.2 \, \mathrm{g \, cm^{-3}}$ is assumed for all spherical and spheroidal particle models. The spheroids are assumed to be randomly oriented; that is, their symmetry axes are uniformly distributed in three-dimensional space. The aspect ratios γ of the spheroids, defined as the ratio of polar to equatorial lengths, are taken to be either 0.5 or 2 to represent oblate and prolate spheroids, respectively. The results of the study show that the scattering properties of the aggregates are fairly well reproduced by an equivalent-mass spheroidal particle when a constant snow density is assumed.

Agreement between the spheroidal/fixed-density model and the aggregates suggests the validity of the simple model and its utility for computing lookup tables for the DPR. An effective snow density of $0.2 \, \mathrm{g \, cm^{-3}}$ is best able to reproduce the scattering parameters of the bullet-rosette aggregates at the DPR frequencies. It is important to note that the effective mass density, as defined in this paper, is that mass density of a spheroidal particle whose associated scattering parameters provide the best match to those of the simulated aggregates with the same mass. This definition is motivated by the desire to match the scattering properties of the spheroidal and simulated aggregates and is distinct from the usual definition of snow density given by the ratio of the particle mass to the volume where the volume is taken to be that of a circumscribing sphere or spheroid. To distinguish our definition from others, the density we use for scattering computations is referred to as the effective snow
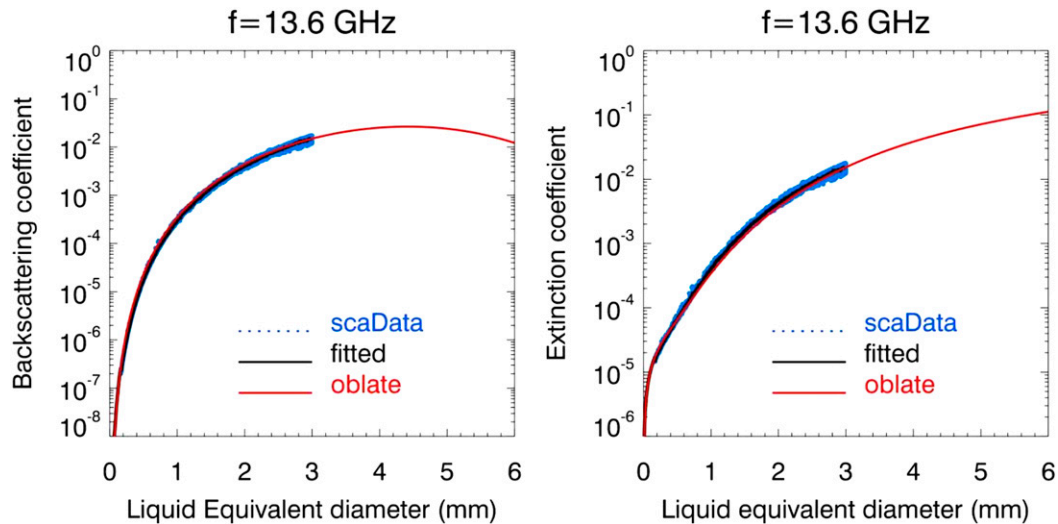
FIG. 2. (left) Backscattering and (right) extinction coefficients from the scattering database (blue dots); simple scattering model (red curves), which is the randomly oriented oblate spheroid with a constant effective density of $0.2 \, \mathrm{g \, cm^{-3}}$ and an aspect ratio of 0.7; and scattering database–simple model combined results (black curves), also referred to as fitted, at Ku band. The mean values of the scattering results are used for the combined results over the data range.

density. It is also important to note that the snow mass is preserved in both definitions; that is, the product of the mass density or the effective mass density and the particle volume yields the same mass.

Recently, Kuo et al. (2016) have developed a comprehensive scattering database, which is computed using the discrete dipole approximation (DDA) from a collection of realistic aggregates simulated from a 3D growth model with mass versus size and fractal properties that are consistent with field observations (Gravner and Griffeath 2009). Because of its limited range of particle sizes mentioned earlier, the scattering tables of snow aggregates in our study will be taken as a hybrid form that combines the scattering results from the Kuo et al. scattering database for small-to-moderate particle sizes and the results from the simple scattering models for large particles. Illustrated in Figs. 2 and 3 are these scattering results at Ku and Ka bands from the Kuo et al. database along with the results from an oblate spheroidal model for particle diameters up to 6 mm. The results from the simple models (red curves) are those obtained from the randomly oriented oblate spheroids with an aspect ratio of 0.7 and a constant effective mass density of $0.2 \, \mathrm{g \, cm^{-3}}$. The results of the scattering tables, which are denoted by the term fitted and shown by the black curves, represent the mean values of the data from the scattering database, where the mean is taken from all types of aggregates having the same mass, and the results from the $0.2 \, \mathrm{g \, cm^{-3}}$ oblate spheroid model in the size range where the scattering database is unavailable. The maximum liquid equivalent diameters of the

current Kuo et al. database at Ku and Ka bands are 3 and 2 mm, respectively. In other words, the scattering results from the simple models are employed in the tables for the size ranges from 3 to 6 mm at Ku band and from 2 to 6 mm at Ka band. The fairly good agreement of the scattering results in Figs. 2 and 3 between the simple model and the scattering database (with mean differences less than 10% for the backscattering and 7% for extinction cross sections) over the size range where the database is valid suggests the validity of the simple models for the smaller particle sizes. As the scattering database is updated to cover larger particle sizes, the validity of the simple scattering model will be reassessed.

b. Particle size/mass distribution model

The three-parameter gamma distribution is one of the most common ways to mathematically describe hydrometeor size/mass distributions (Gorgucci et al. 2000, 2002; Bringi et al. 2002). The form of the gamma distribution is expressed as

$$N(D) = N_W f(\mu) \left(\frac{D}{D_m} \right)^\mu \exp(-\Lambda D), \qquad (1)$$

where D_m is the mass-weighted diameter of the particle, N_w is a scale factor, and μ is the shape factor, where

$$f(\mu) = \frac{6(4 + \mu)^{\mu+4}}{4^4 \Gamma(\mu + 4)} \quad \text{and} \quad \Lambda = (4 + \mu)/D_m. \quad (2)$$
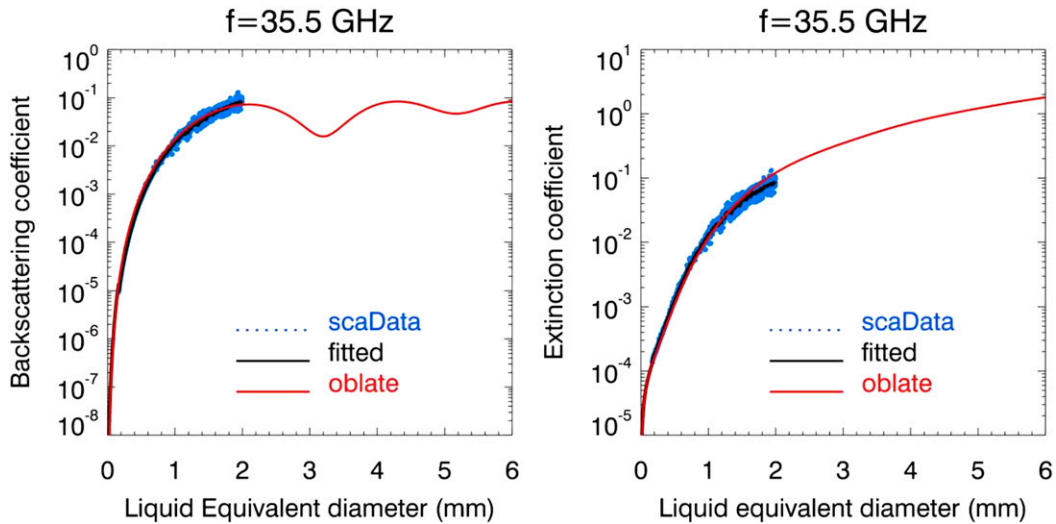
FIG. 3. As in Fig. 2, but for Ka band.

To describe snow particle size and mass spectra, the PSD in (1) and (2) is given as a function of liquid equivalent or melted diameter D, which is also called the particle melted size distribution. We define D_m as the melted median mass diameter:

$$D_m = \frac{\int_0^\infty D^4 N(D)\,dD}{\int_0^\infty D^3 N(D)\,dD}. \tag{3}$$

In the inner swath, the DPR provides Ku- and Ka-band reflectivity factor measurements at each range gate so only two parameters of the PSD can be determined. Typically, the shape factor μ is taken to be constant. Although μ is often set to zero (exponential distribution) (Gunn and Marshall 1958), the impact of this choice on the retrieval needs to be investigated.

The differential frequency ratio (DFR), which is defined as the difference between the radar reflectivity factors at Ku and Ka bands in decibels, is perhaps the most important quantity for the dual-wavelength radar techniques in estimating hydrometeor micro/macrophysical properties. As the DFR is independent of N_w, D_m can be derived from the DFR relations once μ has been fixed. However, the DFR–D_m relation depends not only on μ but on the particle shape, orientation distribution, and mass density. Figure 4 provides the results of DFR as a function of the liquid equivalent median mass diameter using a randomly oriented, fixed-density spheroidal particle model. The left panel in Fig. 4 shows the variations in the DFR–D_m relation resulting from different effective snow densities. Computations of the radar scattering parameters at different effective snow densities are made in the same way as in the case of $0.2\,\mathrm{g\,cm^{-3}}$. The particle sizes (semiaxes of spheroids) are solely determined by the density specified for a given particle mass. The center plot in Fig. 4 shows the effects of a particle's shape, where a γ value of 1 corresponds to a sphere while γ values less than 1 correspond to an oblate spheroid. The plot on the right shows the effects of changing μ. Analysis of these results indicates that particle shape has a small effect on the DFR–D_m relation and changes the results by less than 4% for changes in γ from 0.5 to 1, while the shape factor leads to a change in the results of no more than 20%. On the other hand, the DFR–D_m relation has a strong dependence on the effective snow density. In other words, the determination of D_m from the DFR is relatively insensitive to μ and to particle shape, if the orientation is random, whereas the relationship is quite sensitive to the effective snow density used for computations of the scattering parameters. As can be seen in Figs. 1–3, the extinction coefficients at both Ku and Ka bands, though in good agreement between the simple model and the scattering database, are small and can usually be neglected. It should be noted that the above conclusions are based on the assumption of random orientation of the aggregates. When this assumption is violated, then the orientation distribution as well as particle shape become important.

Although an effective snow density of $0.2\,\mathrm{g\,cm^{-3}}$ is found to be suitable for the computations of the Ku- and Ka-band radar scattering parameters for equivalent ice diameters up to 2–3 mm, further testing will be necessary to assess this assumption when scattering
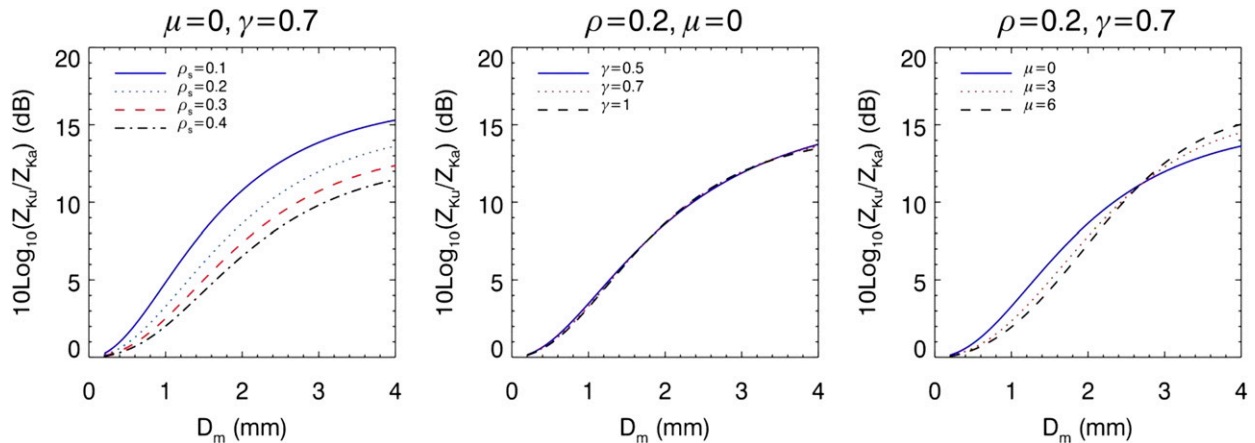
FIG. 4. DFR = $10 \log_{10}(Z_{Ku}/Z_{Ka})$ as a function of equivalent liquid median mass diameter D_m. (left) DFR–D_m relations are plotted with several effective ρ_s from 0.1 to 0.4 g cm^{-3}, as the μ of the gamma PSD is set to zero and the γ of the oblate spheroid particles is set to 0.7. (center) DFR–D_m relations are plotted with the aspect ratios of 0.5, 0.7, and 1 at $\rho_s = 0.2$ g cm^{-3} and $\mu = 0$. (right) DFR–D_m relations are plotted with the values of μ of 0, 3, and 6 at $\rho_s = 0.2$ g cm^{-3} and $\gamma = 0.7$.

results from larger aggregates become available. It is worth noting that the results of Liao et al. (2013) show reasonably good agreement between radar scattering parameters at higher frequencies (from 89 to 183.31 GHz), as derived from the simple models and the simulated aggregates for particle diameters up to 2.5 mm, despite the fact that the simple models using spheres or nearly spherical particles produce back-scattering results with more pronounced oscillations (resonance effects) than do the aggregate results. This is encouraging in the sense that it shows that an effective density of 0.2 g cm^{-3} yields good agreement with the simulated aggregate results for electrically larger particles. On the other hand, it might be the case that the effective snow density may need to be changed for larger particle types so as to ensure good agreement. In either case, the objective is to provide scattering tables at all relevant frequencies and particle sizes that incorporate the most recent scattering results.

c. Dual-wavelength retrieval algorithm

As discussed above, D_m can be derived from the DFR–D_m relations for a given μ. In principle, once D_m is determined, N_w is derived using the radar reflectivity in either the Ku or Ka band. Subsequently, the snow water content (SWC) and equivalent snowfall rate R_S can be computed from the derived PSD parameters. The fall velocity of snow is needed in order to estimate R_S. For the development of an effective dual-wavelength radar retrieval technique, it is desirable to employ lookup tables (LUTs) that are formed in such a way that the radar measurements are directly linked to the microphysical properties of snow

(D_m and N_w) and its associated bulk parameters (SWC and R_S). With use of the LUTs, different particle models and their scattering properties can be evaluated separately within the context of the same algorithm.

Illustrated in Fig. 5 are such tables in which SWC (top left), R_S (top right), D_m (bottom left), and N_w (bottom right) along the ordinate are given as a function of the DFR. A flowchart is provided in Fig. 6 showing the procedures for computing the radar reflectivity factors and snow size and bulk hydrometeor parameters from an assumed mass spectrum model. In Fig. 5, SWC, R_S, and N_w have been normalized by the Ku-band radar reflectivity factor so that they can be expressed solely as a function of DFR for given PSD and scattering model. This method of normalizing liquid water content by reflectivities has previously been adopted in the study of ice clouds (Hogan et al. 2000; Botta et al. 2013). The results in Fig. 5 are computed under the assumption that the snow particles are fixed-density, randomly oriented oblate spheroids with an aspect ratio of 0.7 that follow an exponential particle size distribution. As an example, and also for reference, tables are plotted in Fig. 5 for effective snow densities varying from 0.05 to 0.5 g cm^{-3}. The terminal velocities of snowflakes used for the computations of R_S are based on the results of Magono and Nakamura (1965). It is important to note that the results from the LUTs shown in Fig. 5 can be used to determine SWC and R_S as they directly link the DPR radar reflectivities to SWC and R_S without the use of the derived PSD parameters.

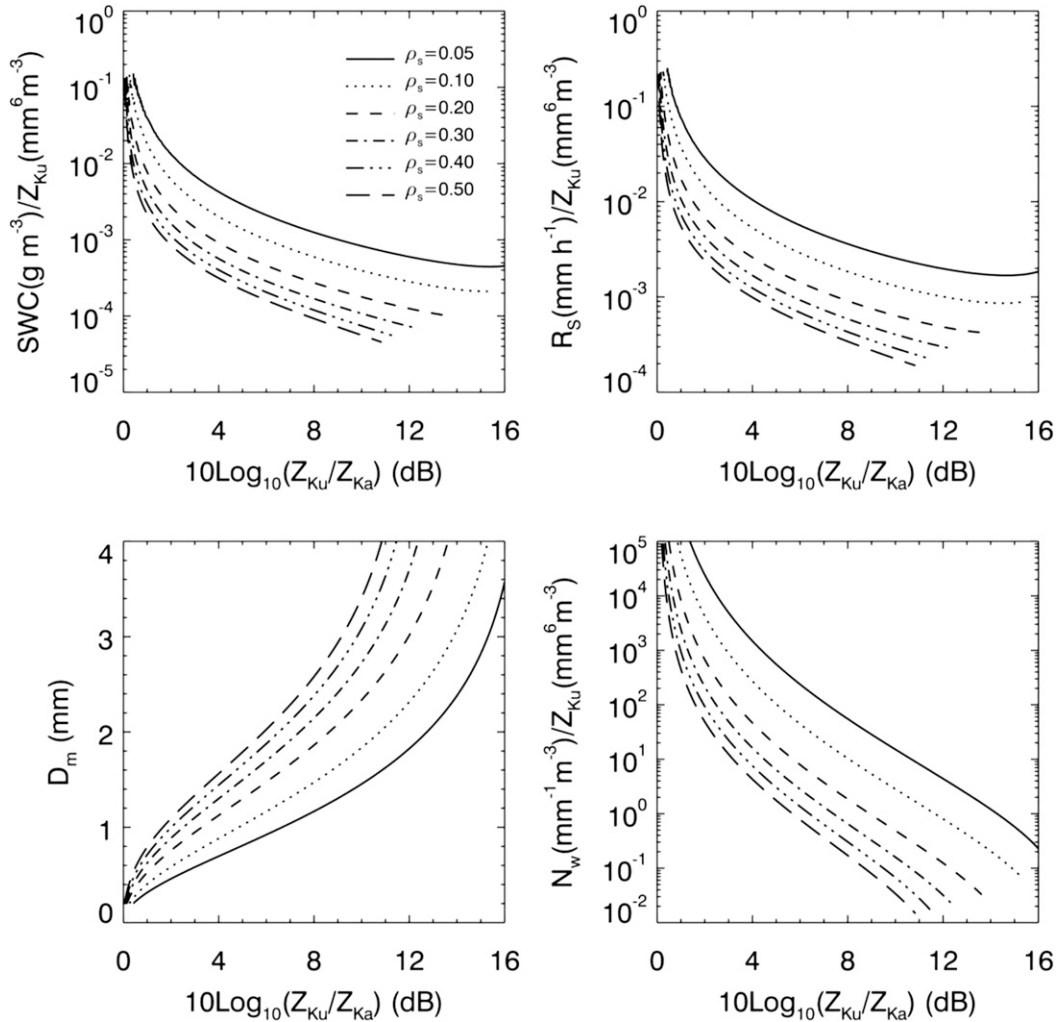The procedure used for estimating snow parameters is described as follows. Given a pair of reflectivity

FIG. 5. The retrieval LUTs that show the (top left) SWC and (top right) R_S, both of which are normalized by Z_{Ku}, as a function of the DFR, defined by $10\log_{10}(Z_{Ku}/Z_{Ka})$, for several effective ρ_s with values from 0.05 to 0.5 g cm^{-3}. (bottom left) The liquid equivalent median mass diameter D_m and (bottom right) the PSD scale parameter N_w normalized by Z_{Ku} are also plotted in terms of DFR.

factors (Z_{Ku}, Z_{Ka}), the DFR (dB) is defined as $10\,\mathrm{Log}_{10}$ (Z_{Ku}/Z_{Ka}), from which we find the values of SWC/Z_{Ku} (Fig.5, top left) and R_S/Z_{Ku} (Fig. 5, top right) for an assumed effective snow density. By multiplying by Z_{Ku}, the results of SWC and R_S are then obtained. Obviously, the values of SWC and R_S depend on the effective snow density. The estimates of D_m and N_w can be achieved in a similar way. It is worth mentioning again that snow attenuations, though correctable, are typically negligibly small for most Ku- and Ka-band spaceborne radar measurements.

As the LUTs change with different scattering models and PSD parameterizations, a proper selection of the tables is critical to the accuracy of the retrieval. It is instructive to conduct a sensitivity study with respect to

the model assumptions and to gain an understanding of the uncertainties associated with each of the models. Figure 7 provides such a sensitivity study in which the LUTs are checked against three μ values. Similar to the findings in Fig. 4, a change in μ leads to changes in the estimates of SWC and R_S of less than 20% so that the assumption of μ equal to zero, as found in many observations, yields a reasonable approximation for the estimates of snow. Although it is worth testing the scattering databases of the aggregates formed from various crystal habits, it is not the focus of the study to evaluate and validate these scattering databases. Because the mass of the aggregates is the dominant factor in the scattering parameters at Ku and Ka bands, significant differences among the various scattering
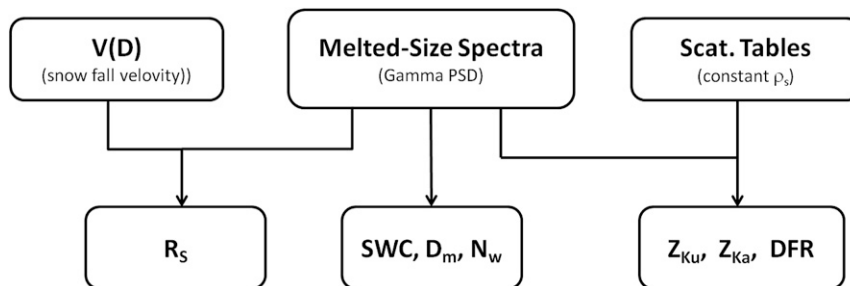
FIG. 6. Flowchart of computing radar parameters and snow size and bulk properties.

databases are not expected. This is evidenced by the fact of that there is good agreement between the scattering databases derived by Nowell et al. (2013) and Kuo et al. (2016) and that the small variations of the scattering and extinction coefficients, as computed from various aggregate models (Kuo et al. 2016), can be seen from the variations in the data (blue) shown in Figs. 2 and 3.

3. Assessment of snow retrieval: PSD model assumptions

Because of the complexity of the snowfall processes and the difficulties encountered in accurately measuring the microphysical properties, validating snow estimates is a challenging task. With the advent of more-advanced digital cameras and image-processing technologies, measurements of falling snow have been improved to the point where the snow particle size spectra and fall velocities can be obtained fairly accurately (Bohm 1989; Huang et al. 2010, 2015; Garrett et al. 2012). An independent and direct measurement of the mass of individual snow particles is, however, still a difficult task, and therefore direct measurements of the snow mass spectrum are rarely available. Several investigations into deriving snow mass spectra are being pursued, which are in fact part of the effort in the GPM ground validation project. These methods are based on the principle that particle masses can be related to their fall velocities after accounting for air drag and other aerodynamics effects (Bohm 1989; Heymsfield et al. 2010). Understanding the microphysical properties of snow should further improve our ability to generate better scattering representations and more accurate lookup tables for retrieving snow bulk properties from the DPR. It would be ideal to evaluate snow retrievals with collocated dual-wavelength radar measurements and in situ snow microphysical measurements. These data, though desirable, are not available. Our attention is therefore focused on the assessment of the PSD assumptions

used in developing the retrieval algorithms employing measured PSD.

To check the consistency of snow retrievals using the LUTs, measurements of snow spectra are examined. The data were obtained from eight snow events during the winter of 2014 taken at the NASA Wallops Flight Facility at Wallops Island, Virginia, using the SVI/PIP. Table 1 provides details of these events that include the starting and ending times of snowfall and the mean temperature, as well as the total accumulations, of each event. At Wallops Island, the annual mean snowfall is about 200.66 mm, and in 2014 it was recorded to be 223.66 mm, slightly more than average. Although the PIP measures the dimensions or sizes of the snowflakes and their fall velocities, it does not provide measurements of particle mass. To compute the radar reflectivities and snow bulk parameters as in (4) and (5) below, the mass spectra or melted size spectra are needed. Conversion of the PSD measurements to the mass spectra, however, relies on the empirical mass–size relations. There are many such relationships available in the literature that can be used to derive $m(D)$ (Nakaya 1954; Magono and Nakamura 1965; Zikmunda and Vali 1972; Locatelli and Hobbs 1974; Mitchell et al. 1990; Brandes et al. 2007; Heymsfield et al. 2010). These results show some variability depending on snow type, amount of riming, and other conditions under which the measurements were made. In this study, two well-known mass–size relations, the results from Heymsfield et al. (2010) and Brandes et al. (2007), are used to test how the estimates of snow change with the use of different mass–size relations when the same LUTs are used.

An example of the PSD measurements is shown in Fig. 8, in which $N(D)$ of the PSD (top), shown along the vertical with the amplitude of the spectrum given by the color scale, is given as a function of time. The equivalent snowfall rate (middle) and median mass diameter D_m (bottom) are also shown in Fig. 8 for the same time period. For the computations of snowfall rate and D_m, empirical snow mass–size relations are used in
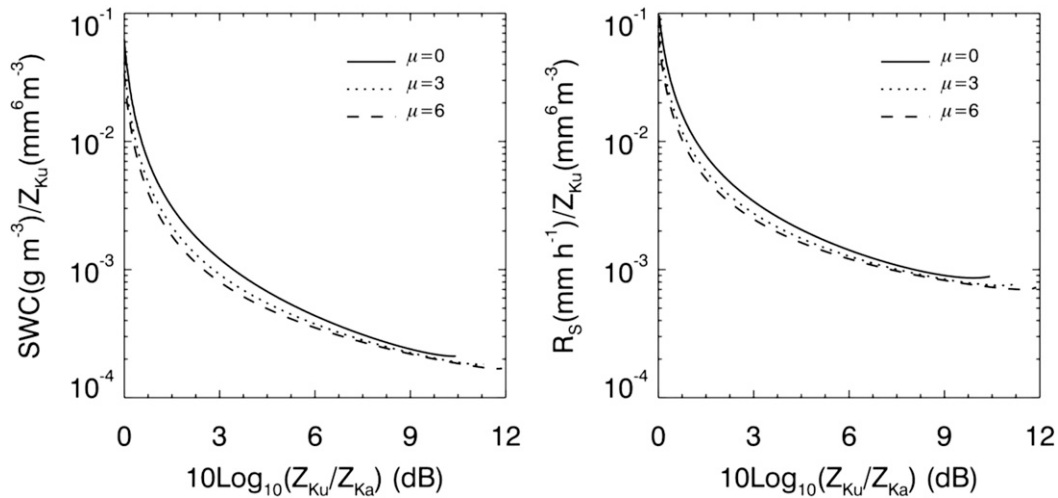
FIG. 7. The LUTs used for the retrieval of (left) SWC and (right) R_S with μ of 0, 3, and 6, respectively, as computed from the single-scattering tables depicted in Figs. 2 and 3.

conjunction with the measured snow particle size spectra and fall velocities. The following equations are used for obtaining R_S and D_m:

$$D_m = \frac{\int_0^\infty Dm(D)N(D)\,dD}{\int_0^\infty m(D)N(D)\,dD} \quad \text{and} \quad (4)$$

$$R_S = \frac{36 \times 10^{-4}}{\rho_w} \int_{D_{\min}}^{D_{\max}} N(D)m(D)V(D)\,dD, \quad (5)$$

where D and D_m in (4) and (5), as well as in Fig. 8, are, respectively, the actual particle diameter and median mass diameter rather than the melted sizes employed in the rest of the paper. The particle mass–size relation is $m(D)$, and ρ_w is the water mass density taken to be $1\,\mathrm{g\,cm^{-3}}$. Note also that the data shown in Fig. 8 represent a measurement period of 1000 min of snow data (~three snow events) with a 1-min integration time. The mass–size relation of Heymsfield et al. (2010) is used for computations of R_S and D_m.

Illustrated in Fig. 9 are the scatterplots (red dots) of SWC (top row) and R_S (bottom row) computed from the measured PSD with use of mass–size relations when the hybrid scattering tables are assumed. For reference, the LUTs derived from the constant effective-density scattering models as shown in Fig. 6 are superimposed in Fig. 9. The SWC and R_S as well as the quantities associated with the Ku- and Ka-band radar reflectivities shown in Fig. 9 are obtained from a total of about 8000 PSD measurements lasting 1 min and collected from the PIP during the winter of 2014 at Wallops Island using the mass–size relations of Brandes et al. (left column) and Heymsfield et al. (right column). Mass–size relations are used to convert the measured PSD to the melted size distribution from which the scattering and snow bulk parameters can be computed as in (2)–(5). The mass–size relations used in Fig. 9 are those from Eq. (8) of Brandes et al. (2007) and from Eq. (10) of Heymsfield et al. (2010). The procedures used in obtaining the radar parameters and SWC and R_S from the measured PSD are shown in the flow diagram in Fig. 10. Analysis of the SWC results indicates that the

TABLE 1. Snow events during the winter of 2014 at Wallops Island.

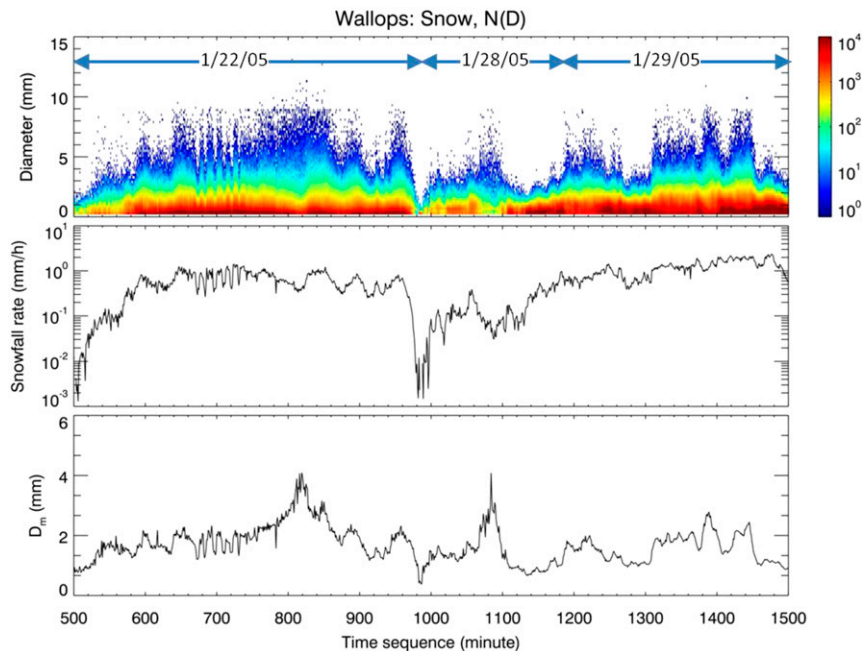| Event	Start time	End time	Accumulation (mm)	Mean temperature (°C)
1	0509 UTC 3 Jan	1130 UTC 3 Jan	46.41	−1.4
2	2205 UTC 21 Jan	1003 UTC 22 Jan	5.52	−5.4
3	2041 UTC 28 Jan	1240 UTC 29 Jan	62.12	−9.5
4	0158 UTC 14 Feb	0512 UTC 14 Feb	6.37	1.9
5	2041 UTC 15 Feb	2323 UTC 15 Feb	0.76	2.2
6	1440 UTC 3 Mar	2200 UTC 3 Mar	34.15	−4.4
7	0804 UTC 17 Mar	2053 UTC 17 Mar	20.93	0.8
8	1850 UTC 25 Mar	0613 UTC 26 Mar	47.40	1.0

FIG. 8. Example of a segment of the PSD measurements (1000 min) in time series taken from eight snow events during the winter of 2014 at the NASA Wallops Flight Facility using SVI/PIP. (top) The particle size spectra ($mm^{-1} m^{-3}$), shown in the color scale, and the (middle) equivalent snowfall rate and (bottom) actual median mass diameter. The PSD data, obtained by averaging the measurements over 1-min integration time, are merged from all the snow events into one data file with consecutive time.

snow water content derived from the measured PSD agrees reasonably well with those from the tables when the effective snow density is taken to be $0.2 \, g \, cm^{-3}$. Because the scattering table, which is a hybrid formed from the mean aggregate solution at small particle sizes and the spheroidal particle model at larger sizes, that is used for computing the reflectivities of the measured PSD and the scattering results with a density of $0.2 \, g \, cm^{-3}$ are nearly the same (as shown in Figs. 2 and 3), the differences in snow water content between the measured PSD and the table results from a density of $0.2 \, g \, cm^{-3}$ are mostly caused by the differences between measured and modeled melted particle size distributions. As noted earlier, the exponential melted-size distribution is assumed in the lookup tables while the measured melted-size distribution is derived from the measured particle diameter spectrum and the mass–size relation that generally will be different from an exponential distribution. Computation of the snowfall rate, on the other hand, depends not only on the particle mass (or melted size) spectrum but also on the particle fall velocities. Most of the estimated snowfall rates, as derived from the measured PSD and the mass–size relations, and shown in the lower panels of Fig. 9, lie between the table results with effective densities of 0.1 and $0.2 \, g \, cm^{-3}$. The mean differences of the SWC between the $0.2 \, g \, cm^{-3}$ snow density

LUTs and the PSD-derived results are about 20% for Ku-band radar reflectivities greater than $15 \, dBZ$ (the approximate minimum detectable signal of the DPR Ku-band channel). Larger differences between the R_S estimates are found and can be attributed to differences in the snowfall velocity spectra between the measured and modeled mass distributions. The terminal velocities of snowflakes used for the computations of the LUTs are based on the results of Magono and Nakamura (1965), while the measured fall velocities are used for the computations of the PSD snowfall rate.

The overall agreement of the snow water content between the results from the measured PSD and the results from the LUTs suggests that the exponential particle distribution model assumed in the tables is reasonable. Different mass–size relations lead to different mass spectra for a given measured PSD. That the retrieval results from the Brandes et al. and Heymsfield et al. mass–size relations follow the trends of SWC and R_S similar to those derived from the LUTs further suggests that the Ku- and Ka-band dual-wavelength techniques adopted are relatively insensitive to the choice of either the Brandes or the Heymsfield mass–size relation. These results approximately yield the table values obtained from the $0.2 \, g \, cm^{-3}$ snow density. It is also worth mentioning that the results from the measured PSD are
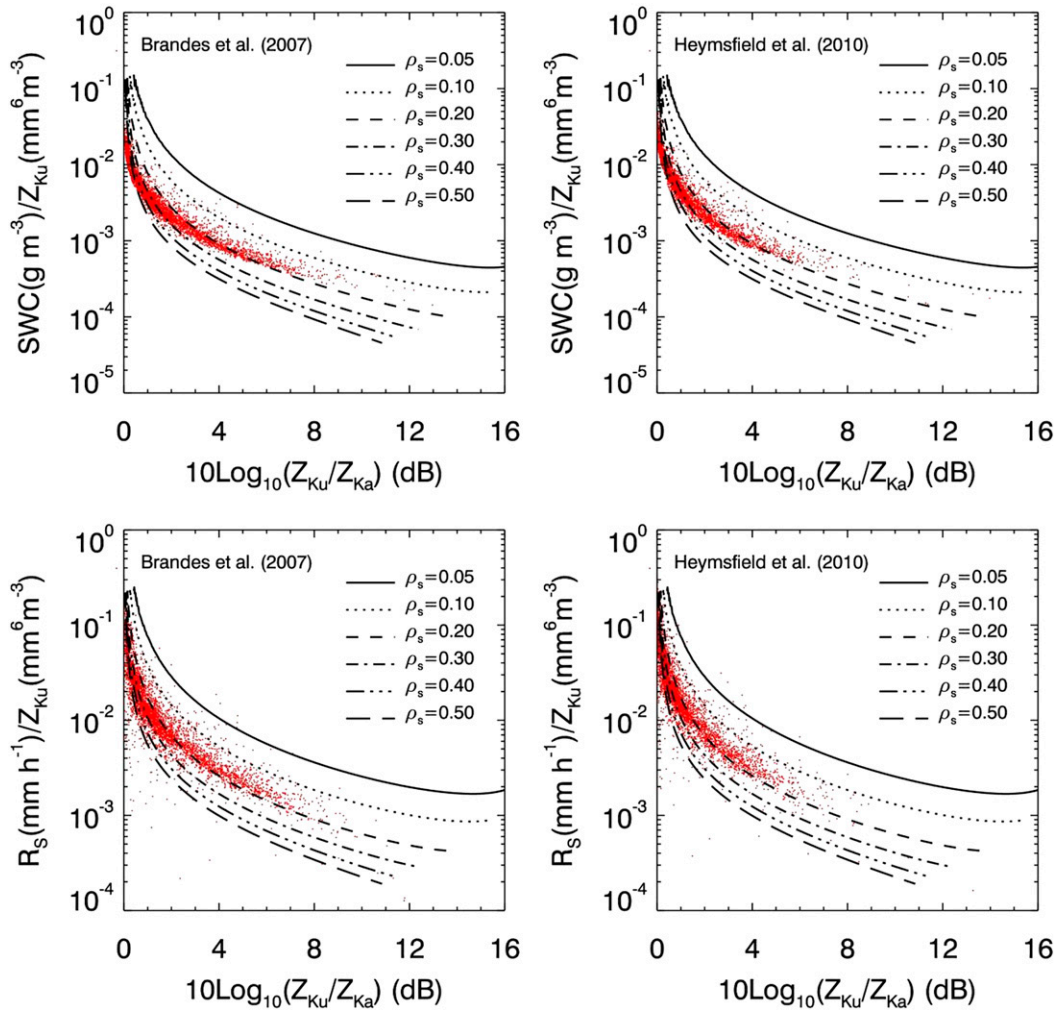
FIG. 9. The (top) SWC and (bottom) R_S, both of which are normalized by Z_{Ku}, as a function of the DFR, defined by $10 \log_{10}(Z_{Ku}/Z_{Ka})$, for several effective ρ_s with the values from 0.05 to 0.5 g cm^{-3}. The scatterplots (red dots) are the results derived from the measured PSD that were collected by SVP/PIP from eight snow events during winter 2014 at the NASA Wallops Flight Facility. Two empirical density–size relationships reported by Brandes et al. (2007) and Heymsfield et al. (2010) are used in converting the measured PSD to the snow mass spectra, and the results from their respective relations are shown in the left and right panels.

relatively insensitive to PSD integration time even though the scatter in the data is slightly reduced if a longer integration is used.

4. Summary

The ultimate goal of this study is to better understand the estimation process in retrieving snow microphysical properties (N_w and D_m) and the associated bulk parameters (SWC and R_S) for improvement of the Ku- and Ka-band dual-frequency radar retrieval. This is done by first finding suitable single-scattering tables and PSD models and then using this information to construct snow retrieval lookup tables. Presently available scattering databases,

though accurate and useful, are limited to small and moderate particle sizes. To extend the results to larger sizes, a simple scattering model that agrees well with the scattering databases at small particle sizes is used. It is found that a snow particle model consisting of randomly oriented oblate spheroids with an effective mass density of 0.2 g cm^{-3} yields good agreement with the results from the scattering databases at Ku and Ka band. Thus, the single-particle scattering database is a hybrid that uses the scattering database for small and moderate particles and a simple randomly oriented oblate with a constant effective mass density of 0.2 g cm^{-3} for large particles.

Using single-scattering tables and an assumed PSD model, the Ku- and Ka-band radar reflectivity factors
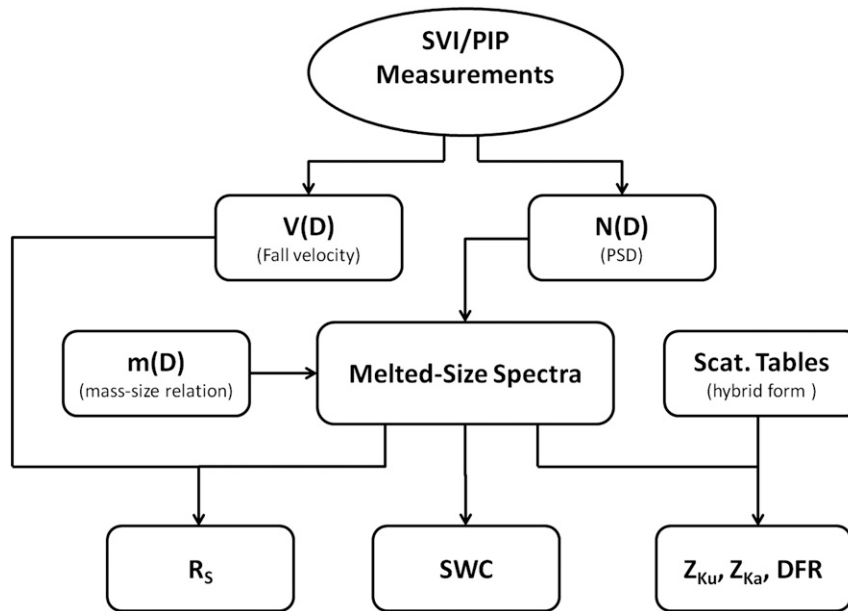
FIG. 10. Flowchart detailing the procedures followed for obtaining radar reflectivities and snow parameters.

and snow bulk parameters are computed. Thus, the relationships between the results of DFR and SWC and R_S are established to form the dual-wavelength radar retrieval lookup tables. Retrievals of snow water content and snowfall rate, as the primary focus of this study, are therefore achieved by using newly introduced lookup tables that directly link Ku- and Ka-band radar reflectivities to hydrometeor parameters without the use of derived PSD parameters. The lookup tables are formed so that SWC and R_S, both of which are normalized by the Ku-band radar reflectivity factor, are expressed as a function of the differential frequency ratio of Ku- and Ka-bands. The lookup tables offer not only computational advantages but provide direct insight into how the model assumptions impact the retrieval results. The nature of one-to-one relations between the normalized hydrometeor parameters and the DFR provides a means for obtaining unique solutions of the snow parameters for a given PSD and single-scattering model. To understand the uncertainties in the snow estimates associated with the PSD parameterizations and scattering models, a sensitivity study was performed, finding that the choice of the shape factor of the gamma PSD has only a slight impact on the retrievals. As such, a value of μ of zero, as supported by some observations, should yield reasonable estimates of snow parameters from the perspective of dual-wavelength radar retrieval.

The self-consistency of the snow retrievals has been checked using measurements of snow PSD and fall velocity acquired from the PIP during the winter of 2014 at Wallops Island. Among several assumptions that have been examined are conversions to particle mass spectra using different mass–size relations, scattering particle models, and snow PSD. Analysis of nearly 8000 PSD measurements lasting 1 min suggests that exponential PSD model ($\mu = 0$) is sufficiently accurate for the dual-wavelength radar retrieval of snow bulk parameters. It also indicates that the use of either the Heymsfield et al. or the Brandes et al. mass–size relation yields approximately the same snow estimates. However, these findings should be viewed as preliminary because of the limited data measurements at a single location. Collections of long-term PSD data, fall velocities, and information on particle mass spectra at multiple sites will assist in the further evaluation of the performance of the Ku- and Ka-band radar techniques. Further tests of the scattering tables will be done by comparing the accuracy of the simple particle model against scattering results from larger simulated aggregates, as these results become available.

APPENDIX

List of Key Symbols and Acronyms Used in This Article

D	Particle diameter
D_m	Mass-weighted diameter
$D_{\min}$	Minimum diameter
$D_{\max}$	Maximum diameter
DDA	Discrete dipole approximation
DFR	Differential frequency ratio
DPR	Dual-Frequency Precipitation Radar
f	Frequency
γ	Aspect ratio of a particle
GPM	Global Precipitation Measurement
JAXA	Japan Aerospace Exploration Agency
Ka band	Frequency of 35.6 GHz
Ku band	Frequency of 13.6 GHz
Λ	Slope parameter
LUT	Lookup table
$m(D)$	Particle mass as a function of particle diameter
μ	Shape factor of the gamma distribution
$N(D)$	Particle size distribution
N_w	Scale factor of the particle size distribution
NASA	National Aeronautics and Space Administration
PSD	Particle size distribution
R_S	Equivalent snowfall rate
ρ_s	Snow mass density
ρ_w	Liquid mass density
SVI/PIP	Snow Video Imager/Particle Image Probe
SWC	Snow water content
$V(D)$	Particle fall velocity
Z_{Ku}	Ku-band radar reflectivity factor
Z_{Ka}	Ka-band radar reflectivity factor

REFERENCES

Bohm, H. P., 1989: A general equation for the terminal fall speed of solid hydrometeors. *J. Atmos. Sci.*, **46**, 2419–2427, doi:10.1175/1520-0469(1989)046<2419:AGEFTT>2.0.CO;2.

Botta, G., K. Aydin, and J. Verlinde, 2010: Modeling of microwave scattering from cloud ice crystal aggregates and melting aggregates: A new approach. *IEEE Geosci. Remote Sens. Lett.*, **7**, 572–576, doi:10.1109/LGRS.2010.2041633.

——, ——, ——, A. E. Avramov, A. S. Ackerman, A. M. Fridlind, G. M. McFarquhar, and M. Wolde, 2011: Millimeter wave scattering from ice crystal aggregates: Comparing cloud model simulations with X- and Ka-band radar measurements. *J. Geophys. Res.*, **116**, D00T04, doi:10.1029/2011JD015909.

——, ——, and ——, 2013: Variability in millimeter wave scattering properties of dendritic ice crystals. *J. Quant. Spectrosc. Radiat. Transfer*, **131**, 105–104, doi:10.1016/j.jqsrt.2013.05.009.

Brandes, E., K. Ikeda, G. Zhang, M. Schoenhuber, and R. Rasmussen, 2007: A statistical and physical description of

hydrometeor distributions in Colorado snowstorms using a video disdrometer. *J. Appl. Meteor. Climatol.*, **46**, 634–650, doi:10.1175/JAM2489.1.

Bringi, V., G. Huang, V. Chandrasekar, and E. Gorgucci, 2002: A methodology for estimating the parameters of a gamma raindrop size distribution model from polarimetric radar data: Application to a squall-line event from the TRMM/Brazil campaign. *J. Atmos. Oceanic Technol.*, **19**, 633–645, doi:10.1175/1520-0426(2002)019<0633:AMFETP>2.0.CO;2.

Draine, B. T., and P. J. Flatau, 1994: Discrete dipole approximation for scattering calculations. *J. Opt. Soc. Amer.*, **11A**, 1491–1499, doi:10.1364/JOSAA.11.001491.

Garrett, T. J., C. Fallgatter, K. Shkurko, and D. Howlett, 2012: Fall speed measurement and high-resolution multi-angle photography of hydrometeors in free fall. *Atmos. Meas. Tech.*, **5**, 2625–2633, doi:10.5194/amt-5-2625-2012.

Gorgucci, E., G. Scarchilli, V. Chandrasekar, and V. Bringi, 2000: Measurement of mean raindrop shape from polarimetric radar observations. *J. Atmos. Sci.*, **57**, 3406–3413, doi:10.1175/1520-0469(2000)057<3406:MOMRSF>2.0.CO;2.

——, ——, ——, and ——, 2002: Estimation of raindrop size distribution parameters from polarimetric radar measurements. *J. Atmos. Sci.*, **59**, 2373–2384, doi:10.1175/1520-0469(2002)059<2373:EORSDP>2.0.CO;2.

Gravner, J., and D. Griffeath, 2009: Modeling of snow-crystal growth: A three-dimensional mesoscopic approach. *Phys. Rev. E*, **79**, 011601, doi:10.1103/PhysRevE.79.011601.

Gunn, K. L. S., and J. S. Marshall, 1958: The distribution with size of aggregate snowflakes. *J. Meteor.*, **15**, 452–461, doi:10.1175/1520-0469(1958)015<0452:TDWSOA>2.0.CO;2.

Heymsfield, A. J., Z. Wang, and S. Matrosov, 2005: Improved radar ice water content retrieval algorithms using coincident microphysical and radar measurements. *J. Appl. Meteor.*, **44**, 1391–1412, doi:10.1175/JAM2282.1.

——, C. Schmitt, A. Bansemer, and C. H. Twohy, 2010: Improved representation of ice particle masses based on observations in natural clouds. *J. Atmos. Sci.*, **67**, 3303–3318, doi:10.1175/2010JAS3507.1.

Hogan, R., A. Illingworth, and H. Sauvageot, 2000: Measuring crystal size in cirrus using 35- and 94-GHz radars. *J. Atmos. Oceanic Technol.*, **17**, 27–37, doi:10.1175/1520-0426(2000)017<0027:MCSICU>2.0.CO;2.

Hou, A. Y., G. S. Jackson, C. Kummerow, and C. M. Shepherd, 2008: Global precipitation measurement. *Precipitation: Advances in Measurement, Estimation, and Prediction*, S. Michaelides, Ed., Springer, 131–169.

——, and Coauthors, 2014: The Global Precipitation Measurement Mission. *Bull. Amer. Meteor. Soc.*, **95**, 701–722, doi:10.1175/BAMS-D-13-00164.1.

Huang, G., V. N. Bringi, R. Cifelli, D. Hudak, and W. A. Petersen, 2010: A methodology to derive radar reflectivity–liquid equivalent snow rate relations using C-band radar and a 2D video disdrometer. *J. Atmos. Oceanic Technol.*, **27**, 637–651, doi:10.1175/2009JTECHA1284.1.

——, ——, D. Moisseev, W. A. Petersen, L. Bliven, and D. Hudak, 2015: Use of 2D-video disdrometer to derive mean density–size and Z_e–SR relations: Four snow cases from the Light Precipitation Validation Experiment. *Atmos. Res.*, **153**, 34–48, doi:10.1016/j.atmosres.2014.07.013.

Kuo, K.-S., and Coauthors, 2016: The microwave radiative properties of falling snow derived from realistic ice particle models. Part I: An extensive database of simulated pristine

crystals and aggregate particles, and their scattering properties. *J. Appl. Meteor. Climatol.*, **55**, 691–708, doi:10.1175/JAMC-D-15-0130.1.

Liao, L., and R. Meneghini, 2005: On modeling air/spaceborne radar returns in the melting layer. *IEEE Trans. Geosci. Remote Sens.*, **43**, 2799–2809, doi:10.1109/TGRS.2005.848704.

——, ——, L. Tian, and G. M. Heymsfield, 2008: Retrieval of snow and rain from combined X- and W-band airborne radar measurements. *IEEE Trans. Geosci. Remote Sens.*, **46**, 1514–1524, doi:10.1109/TGRS.2008.916079.

——, ——, H. Nowell, and G. Liu, 2013: Scattering computations of snow aggregates from simple geometrical particle models. *IEEE J. Sel. Top. Earth Obs. Remote Sens.*, **6**, 1409–1417, doi:10.1109/JSTARS.2013.2255262.

Liu, G., 2004: Approximation of single scattering properties of ice and snow particles for high microwave frequencies. *J. Atmos. Sci.*, **61**, 2441–2456, doi:10.1175/1520-0469(2004)061<2441:AOSSPO>2.0.CO;2.

——, 2008: A database of microwave single-scattering properties for nonspherical ice particles. *Bull. Amer. Meteor. Soc.*, **89**, 1563–1570, doi:10.1175/2008BAMS2486.1.

Locatelli, J., and P. Hobbs, 1974: Fall speeds and masses of solid precipitation particles. *J. Geophys. Res.*, **79**, 2185–2197, doi:10.1029/JC079i015p02185.

Magono, C., and T. Nakamura, 1965: Aerodynamic studies of falling snowflakes. *J. Meteor. Soc. Japan*, **43**, 139–147.

Matrosov, S. Y., 1998: A dual-wavelength radar method to measure snowfall rate. *J. Appl. Meteor.*, **37**, 1510–1521, doi:10.1175/1520-0450(1998)037<1510:ADWRMT>2.0.CO;2.

——, A. J. Heymsfield, and Z. Wang, 2005: Dual-frequency ratio of nonspherical atmospheric hydrometeors. *Geophys. Res. Lett.*, **32**, L13816, doi:10.1029/2005GL023210.

Mitchell, D. L., R. Zhang, and R. L. Pitter, 1990: Mass-dimensional relations for ice particles and the influence of riming on snowfall rates. *J. Appl. Meteor.*, **29**, 153–163, doi:10.1175/1520-0450(1990)029<0153:MDRFIP>2.0.CO;2.

Nakaya, U., 1954: *Snow Crystals: Natural and Artificial*. Harvard University Press, 510 pp.

Newman, A., P. A. Kucera, and L. Bliven, 2009: Presenting the Snow Video Imager (SVI). *J. Atmos. Oceanic Technol.*, **26**, 167–179, doi:10.1175/2008JTECHA1148.1.

Nowell, H., G. Liu, and R. Honeyager, 2013: Modeling the microwave single-scattering properties of aggregate snowflakes. *J. Geophys. Res. Atmos.*, **118**, 7873–7885, doi:10.1002/jgrd.50620.

Petty, G. W., and W. Huang, 2010: Microwave backscattering and extinction by soft ice spheres and complex snow aggregates. *J. Atmos. Sci.*, **67**, 769–787, doi:10.1175/2009JAS3146.1.

Seto, S., T. Iguchi, and T. Oki, 2013: The basic performance of a precipitation retrieval algorithm for the Global Precipitation Measurement Mission's single/dual-frequency radar measurements. *IEEE Trans. Geosci. Remote Sens.*, **51**, 5239–5251, doi:10.1109/TGRS.2012.2231686.

Szyrmer, W., and I. Zawadzki, 2014a: Snow studies. Part III: Theoretical derivations for the ensemble retrieval of snow microphysics from dual-wavelength vertically pointing radars. *J. Atmos. Sci.*, **71**, 1158–1170, doi:10.1175/JAS-D-12-0285.1.

——, and ——, 2014b: Snow studies. Part IV: Ensemble retrieval of snow microphysics from dual-wavelength vertically pointing radars. *J. Atmos. Sci.*, **71**, 1172–1186.

Wang, Z., G. M. Heymsfield, L. Li, and A. J. Heymsfield, 2005: Retrieving optically thick ice cloud microphysical properties by using airborne dual-wavelength radar measurements. *J. Geophys. Res.*, **110**, D19201, doi:10.1029/2005JD005969.

Weinman, J., and M.-J. Kim, 2007: A simple model of the millimeter-wave scattering parameters of randomly oriented aggregates of finite cylindrical ice hydrometeors. *J. Atmos. Sci.*, **64**, 634–644, doi:10.1175/JAS3841.1.

Zikmunda, J., and G. Vali, 1972: Fall patterns and fall velocities of rimed ice crystals. *J. Atmos. Sci.*, **29**, 1334–1347, doi:10.1175/1520-0469(1972)029<1334:FPAFVO>2.0.CO;2.